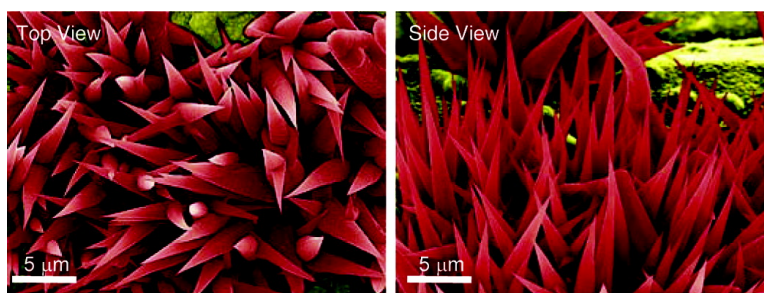## Communication

Diamond-Hexagonal Semiconductor Nanocones with Controllable Apex Angle

Linyou Cao, Lee Laim, Chaoying Ni, Bahram Nabet, and Jonathan E. Spanier

More About This Article

Additional resources and features associated with this article are available within the HTML version:

- Supporting Information
- Links to the 5 articles that cite this article, as of the time of this article download
- Access to high resolution figures
- Links to articles and content related to this article
- Copyright permission to reproduce figures and/or text from this article

View the Full Text HTML

Diamond-Hexagonal Semiconductor Nanocones with Controllable Apex Angle

Linyou Cao,[†] Lee Laim,[†] Chaoying Ni,[‡] Bahram Nabet,[§,†,⊥] and Jonathan E. Spanier[*,†,§,⊥]

Department of Materials Science and Engineering, Department of Electrical and Computer Engineering, A. J. Drexel Nanotechnology Institute, Drexel University, Philadelphia, Pennsylvania 19104, and Department of Materials Science and Engineering and the W. M. Keck Electron Microscopy Facility, University of Delaware, Newark, Delaware 19716

Received July 6, 2005; E-mail: spanier@drexel.edu

Control of nanocrystal topology and of the formation of selected polymorphs is an important feature for fundamental studies of crystal growth and for investigating the shape and structural dependence of many properties.[1] Such control is also critical in developing new pathways for materials synthesis[2] and new applications of nanostructured materials.[3]

Conical nanostructures of carbon,[4a] BN,[4b] AlN,[4c] SiC,[4d] ZnO,[4e] and Si[4f−g] have attracted interest recently because of their potential uses in field emission, in nanoscaled manipulation, and as scanning probe microscopy and near-field scanning optical microscopy probes. Tapered nanostructures are expected to have higher bending stiffness than nanotubes and nanowires and better resistance to thermal-induced drift than nanowires.[5] Shape engineering of properties represents an important design flexibility for these and other applications.[6]

Silicon-based nanostructures produced by bottom-up methods are highly attractive as key elements in emerging nanoelectronic device technologies due to performance superior to current top-down fabricated Si-based commercial devices and its cost-effectiveness for developing large-scaled electronic circuits.[7] Despite the number of polymorphs in bulk Si, nanostructured silicon materials produced by bottom-up methods have been limited to the diamond-cubic (DC) structure.[8] Here, we report the metal-catalyzed chemical vapor deposition synthesis of Si and Ge solid nanocones (SiNCs, GeNCs) with control of apex angles. Significantly, we also find that the structure of the SiNCs is not the conventional DC phase, but rather diamond-hexagonal (DH).

Evaporated and annealed 2 nm thick Au films or 2−30 nm diameter Au colloids (Ted Pella) cast on poly-L-lysine-functionalized SiO_2-coated Si(100) substrates were exposed to flowing precursor of 10% SiH_4 in He, ∼20−200 sccm (10% GeH_4 in He, ∼50 sccm), and carrier gas of N_2 or 5% H_2 in Ar, ∼100 sccm (∼50 sccm) at 650 °C (400 °C) under ∼20 Torr (∼400 Torr) for synthesis of SiNCs (GeNCs) in a quartz tube furnace for 5−150 min. The resulting SiNCs and GeNCs were characterized by scanning electron microscopy (SEM, FEI-XL30), energy-dispersive X-ray spectroscopy (EDS), transmission electron microscopy (TEM, JEOL 2010F), and Raman scattering spectroscopy (Renishaw 1000). TEM samples were prepared by sonicating the SiNCs and GeNCs from growth substrates in ethanol and dropping onto Ni or Cu TEM grids.

Figure 1a shows an SEM image of a representative yield of SiNCs; the insets show a TEM image of a SiNC tip with a catalyst particle (upper) and an SEM of the hexagonal cross-section of a SiNC (lower). The SiNCs shown are ∼10 μm long, ∼2 μm wide at the base, and the typical tip radius r_{tip} of the SiNC is ∼5 nm,
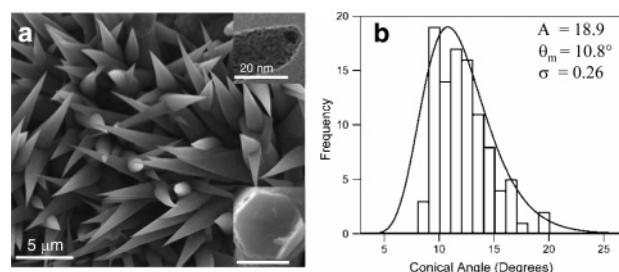

Figure 1. (a) SEM image of an array of silicon nanocones (SiNCs). Upper inset: a representative TEM image of one SiNC tip showing the Au nanoparticle at the tip. Lower inset: the hexagonal cross-section of a SiNC with a scale bar of 1 μm. (b) Distribution of conical angles and log-normal fitting curve with fitting parameters identified in the text.

though some possess catalyst-free tips with $r_{tip} \approx 1−2$ nm (not shown). Similar results were obtained with GeNCs (see Supporting Information). EDS analysis performed in TEM and SEM (not shown) confirms that each SiNC consists of Si throughout the structure. In addition, the SiNCs possess a relatively narrow distribution of conical angles (Figure 1b). This distribution can be fitted by a log-normal function $F(\theta) = A \exp[-\ln^2(\theta/\theta_m)/2\sigma^2]$ using the method of least squares, where the fitting parameters A, θ_m, and σ correspond to the fraction of SiNCs with the most probable apex angle, the most probable apex angle, and the width of the distribution, respectively; such a distribution is observed often in the morphology of nanoscale materials.[8c]

Images a and b of Figure 2 show a representative TEM image of a SiNC and the selected area electron diffraction (SAED) which was collected from the area indicated by the circle in Figure 2a, respectively. Shown in the inset of Figure 2b is the defocusing diffraction-mode image of the same area where SAED was collected. This diffraction pattern indicates hexagonal symmetry, and it can be indexed as a superposition of [0001] and [1̄2̄30] zone axis patterns from the DH structure. These zone axis patterns possess common ⟨1̄21̄0⟩ reflections, and analysis demonstrates that the axial direction of this SiNC is [1̄2̄1̄0], as illustrated in Figure 2b. In addition, Figure 2c shows a HRTEM image of the [21̄1̄0] projection of the SiNC, which is in good accordance with the modeling view for DH silicon shown in its inset. (Those Si atoms which are colored gray in the model cannot be observed clearly in the HRTEM image due to limits of instrument resolution.) A different type of diffraction pattern is also observed (Figure 2d). This pattern can be indexed as superposition of [011̄1] and two ⟨201⟩ ([202̄1] and [022̄1]) zone patterns of DH Si (see Supporting Information). From these HRTEM and electron diffractions, the lattice constants are determined to be $a = 3.82$ Å and $c = 6.22$ Å, with $c/a = 1.63$; these values are consistent with those reported in DH silicon film (see Supporting Information).[8a,b] We believe the formation of DH silicon phase is due to stacking faults on {111}$_{cubic}$
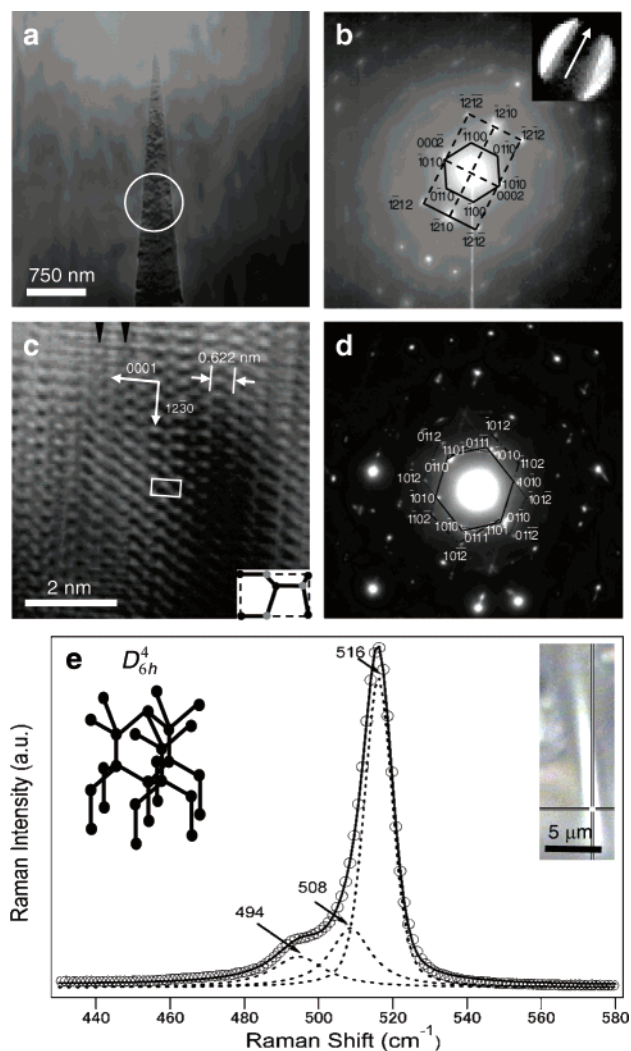
Figure 2. (a) TEM image of a SiNC, (b) corresponding selected area electron diffraction (SAED) pattern consisting of [0001] and [2$\bar{1}$30] zone diffraction collected from area denoted by circle in (a). Inset: defocusing diffraction-mode image of selected area with white arrow indicating axial direction within this SiNC. (c) High-resolution transmission electron microscopy (HRTEM) image of the [2$\bar{1}$10] projection of SiNCs. Inset: model of projective view along [2$\bar{1}$10] direction; the black arrows indicate the planes along which stacking faults exist. (d) SAED pattern consisting of ⟨011⟩ and two ⟨201⟩ zone diffraction. (e) The Raman spectrum of a SiNC (circles), including a multiple peak fitting (solid line) and the deconvolved line shapes (dashed lines). Left inset: structural model for DH silicon. Right inset: optical image shows area from which the Raman spectrum is collected.

planes as shown by black arrows in Figure 2c. Change in the atomic sequence of the neighboring $\{111\}_{cubic}$ planes from ABCABC to ABABAB corresponds to a change in the structure of Si from DC to DH.

The structure of the SiNCs was also characterized by Raman scattering in the backscattering configuration using a HeNe laser ($\lambda = 632.8$ nm) with an incident power of $\sim$2.8 mW focused to $\sim$1 μm. Figure 2e shows a typical Raman spectrum collected from a single SiNC and the corresponding multiple peak-fitting of the line shape. Whereas the DC phase of Si exhibits a degenerate optical phonon peak at $\sim$520 cm^{-1}, the fitted Raman spectrum of our SiNCs contains three peaks in this region of the spectrum. These fitted peak energies (irreps)— $\sim$516 (A_{1g}), $\sim$509 (E_{1g}), and $\sim$494
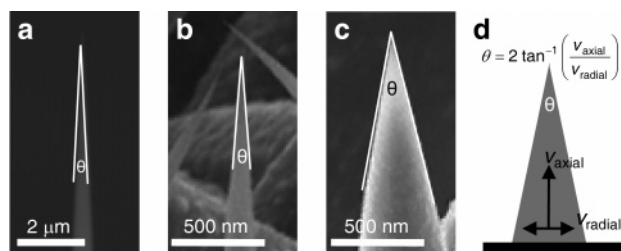

Figure 3. Representative SEM images of SiNCs produced using (a) 2 nm Au film, (b) 20 nm diameter and (c) 2 nm Au colloids. These SiNCs possess conical angles $6.4 \pm 0.8°$, $9.0 \pm 2.0°$, and $20.0 \pm 3.6°$, respectively. (d) Schematic model for the growth of SiNC.

(E_{2g}) cm^{-1}—are in excellent agreement with theoretically calculated, Γ-point Raman-active phonon energies for DH−Si.[9] The presence of the E_{2g} mode is further evidence of the DH structure of our SiNCs.

Finally, we demonstrate tunability of the apex angle of SiNCs using catalysts of different sizes. As shown in Figure 3a−c, decreasing the catalyst size from $\sim$50 nm (obtained by thermal pretreatment of the 2 nm thick film) to $\sim$2 nm results in a concomitant increase in the apex angle (Supporting Information). The apex angle is determined by the relative rates of radial and axial growth, as illustrated in Figure 3d. The selective influence of catalyst nanoparticle size on axial growth rate as reported for nanowires[10] likely plays a significant role in the controlled variation of apex angles. We hope that this work will generate further interest in and enable more detailed investigations of the shape- and structure-dependent properties of semiconductor nanocones.

Supporting Information Available: (1) SEM of GeNCs; (2) schematic model for DH silicon structure and indexing of SAED patterns; (3) histograms of conical angles of SiNCs. This material is available free of charge via the Internet at http://pubs.acs.org.

References

(1) Moriarty, P. *Rep. Prog. Phys.* **2001**, *64*, 297.
(2) Manna, L.; Milliron, D. J.; Meisel, A.; Scher, E. C.; Alivisatos, A. P. *Nat. Mater.* **2003**, *2*, 382.
(3) Law, M.; Goldberger, J.; Yang, P. *Annu. Rev. Mater. Res.* **2004**, *34*, 83.
(4) (a) Zhang, G. Y.; Jiang, X.; Wang, E. G. *Science* **2003**, *300*, 472. (b) Azevedo, S.; Mazzoni, M. S. C.; Chacham, H.; Nunes, R. W. *Appl. Phys. Lett.* **2003**, *82*, 2323. (c) Liu, C.; Hu, Z.; Wu, Q.; Wang, X. Z.; Chen, Y.; Sang, H.; Zhu, J. M.; Deng, S. Z.; Xu, N. S. *J. Am. Chem. Soc.* **2005**, *127*, 1318. (d) Lin, M.; Loh, K. P.; Boothroyd, C.; Du, A. Y. *Appl. Phys. Lett.* **2004**, *85*, 5388. (e) Han, X.; Wang, G.; Jie, J.; Choy, W. C. H.; Luo, Y.; Yuk, T. I.; Hou, J. G. *J. Phys. Chem. B* **2005**, *109*, 2733. (f) Sharma, S.; Kamins, T. I.; Williams; R. S. *J. Cryst. Growth* **2004**, *267*, 613. (g) Bai, X. D.; Zhi, C. Y.; Liu, S.; Wang, E. G.; Wang, Z. L. *Solid State Commun.* **2003**, *125*, 185.
(5) Wei, C.; Srivastava, D. *Appl. Phys. Lett.* **2004**, *85*, 2208.
(6) Terrones, H.; Terrones, M. *New J. Phys.* **2003**, *5*, 126.
(7) Cui, Y.; Zhong, Z.; Wang, D.; Wang, W. U.; Lieber, C. M. *Nano Lett.* **2003**, *3*, 149.
(8) (a) Hendirks, M.; Radelaar, S.; Beers, A. M.; Bloen, J. *Thin Solid Films* **1984**, *113*, 59. (b) Cerva, H. *J. Mater. Res.* **1991**, *11*, 2324. (c) Adu, K. W.; Gutierrez, H. R.; Kim, U. J.; Sumanasekera, G. U.; Eklund, P. C. *Nano Lett.* **2005**, *5*, 409.
(9) Wu, B. R. *Phys. Rev. B* **2001**, *61*, 5.
(10) Kikkawa, J.; Ohno, Y.; Takeda, S. *Appl. Phys. Lett.* **2005**, *86*, 123109.

JA0544814